Nonlinearity management of photonic composites and observation of spatial-modulation instability due to quintic nonlinearity

Albert S. Reyna* and Cid B. de Araújo
Departamento de Física, Universidade Federal de Pernambuco, 50670-901, Recife, PE, Brazil
(Received 11 February 2014; published 10 June 2014)

We present a procedure for nonlinearity management of metal-dielectric nanocomposites (MDNCs). Varying the volume fraction occupied by silver nanoparticles (NPs) suspended in acetone we could investigate the nonlinear (NL) response of the MDNC. In particular, we could cancel the NL refractive index related to the effective third-order susceptibility, $\chi^{(3)}_{\rm eff}$, and thus the NL refractive behavior of the MDNC was due to the effective fifth-order susceptibility, $\chi^{(5)}_{\rm eff}$. Hence, in a cross-phase modulation experiment, we demonstrated the effect of spatial-modulation instability due to $\chi^{(5)}_{\rm eff}$. The experimental results are corroborated with numerical calculations based on a generalized Maxwell-Garnet model that includes the direct contributions of the NPs and the host medium as well as cascade contributions due to the third- and fifth-order susceptibilities of the NPs.

DOI: 10.1103/PhysRevA.89.063803 PACS number(s): 42.65.An, 42.65.Jx, 78.67.Bf

I. INTRODUCTION

The nonlinear (NL) response of matter to optical fields can be described by expressing the induced polarization by a power series of the field with NL susceptibilities, $\chi^{(N)}$, $N = 2, 3, \ldots$, as coefficients of the series [1]. Since all even-order susceptibilities are null in systems with inversion symmetry, the lowest-order NL response in centrosymmetric systems is generally due to the third-order susceptibility, $\chi^{(3)}$, which contributes for generation of fields that depend on the cubic power of the incident field. Therefore, most of the NL studies reported are related to $\chi^{(3)}$ that is responsible for two-photon absorption, third-harmonic generation, and coherent Raman scattering, among other effects. Cascade processes of $\chi^{(3)}$ behave analogously to high-order nonlinearities (HON) processes and were reported for gases and condensed matter systems [2]. Nevertheless, experiments based on HON, related to direct (not-cascade) processes, have been reported for a large variety of physical systems [3].

HON are still under investigation from the fundamental point of view [4] and there is large interest in phenomena such as liquid light condensates [5], soliton formation [6,7], and other transverse NL effects [7,8]. Interferences between third- and fifth-order processes were reported for different systems [9]. Also of interest is the exploitation of HON in quantum information [10], quantum memories [11], and for improvement of high-precision measurements [12].

The interest in effects related to quintic and cubic-quintic nonlinearities has led several authors to investigate theoretically new NL phenomena and propose experiments with metal-dielectric nanocomposites (MDNCs) [7]. From the basic point of view MDNCs are interesting systems because their NL response can be controlled by changing the nanoparticles (NPs) volume fraction, f—the ratio between the volume occupied by the NPs and the host. Indeed, the interest in the NL properties of MDNC is large in nanoscience and nanotechnology [13–18].

In this paper we present a procedure for nonlinearity management of a MDNC aiming its exploitation for practical realization of mathematical models and experiments related to HON [7,19]. The NL response of a colloid consisting of silver NPs suspended in acetone was described by effective susceptibilities, $\chi^{(2N+1)}_{\rm eff}$, $N = 1, 2, 3, \ldots$, that depend on the NL susceptibilities of the host liquid and NPs. HON up to seventh order were measured as a function of the NP volume fraction. In particular for $f = 1.6 \times 10^{-5}$ we obtained $\mathrm{Re}\chi^{(3)}_{\rm eff} = 0$ and $\mathrm{Re}\chi^{(5)}_{\rm eff} \neq 0$ with negligible values of $\mathrm{Im}\chi^{(3)}_{\rm eff}$ and $\mathrm{Im}\chi^{(5)}_{\rm eff}$. Using this condition two-beam cross-phase modulation experiments were performed and revealed the effect of spatial-modulation instability (SMI) due to the fifth-order susceptibility. The third-order SMI effect is well known but the effect due to only $\chi^{(5)}_{\rm eff}$ was not reported before.

II. EXPERIMENTAL DETAILS

The silver colloid was prepared as described in [13,20]: 90 mg of $AgNO_3$ were diluted in 500 ml of water at 100 °C; 10 ml of solution of 1% sodium citrate was added for reducing the Ag^+ ions, and later was boiled and strongly stirred for 1 h. Subsequently, photofragmentation of the NPs [21] was performed by placing a cuvette containing the pristine colloid in front of the second harmonic beam from a Q-switched Nd:YAG laser (10 Hz, 8 ns, 85 mJ/pulse) for 1 h while the suspension was slowly stirred. A homogeneous distribution of spherical NPs (average diameter: 9.0 ± 2.2 nm) was obtained. Hence, colloids prepared by adding 20–300 μl of the Ag-water suspension in 1 ml of acetone, with f varying from 0.5×10^{-5} to 2.5×10^{-4}, were used in the experiments.

The linear absorption spectra of the samples were measured using a commercial spectrophotometer. For the NL measurements we used the second harmonic of a Q-switched and mode-locked Nd: YAG laser (80 ps, 532 nm); single pulses at 10 Hz were selected using a pulse picker. The incident pulses on the samples had maximum energy of 10 μJ.

III. RESULTS AND DISCUSSION

Figure 1 shows the absorption spectra of the colloid before (pristine) and after photofragmentation of the NPs using 8-ns pulses with 85 mJ/each at 532 nm. The fragmentation

*Corresponding author: areynao@yahoo.com.br

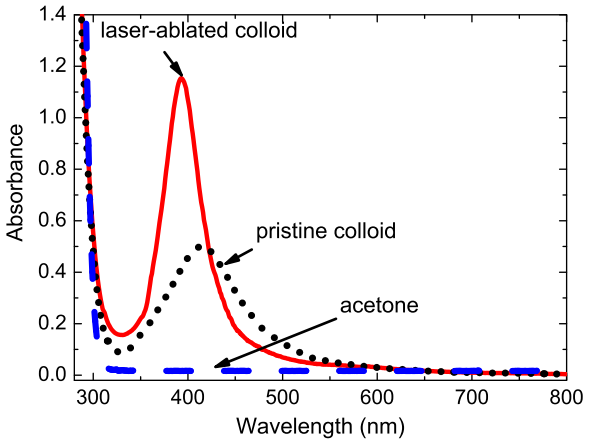

FIG. 1. (Color online) Linear absorption spectra of acetone (dashed line) and silver colloid before (dotted line) and after photofragmentation of the NPs (solid line). Cell length: 1 mm.

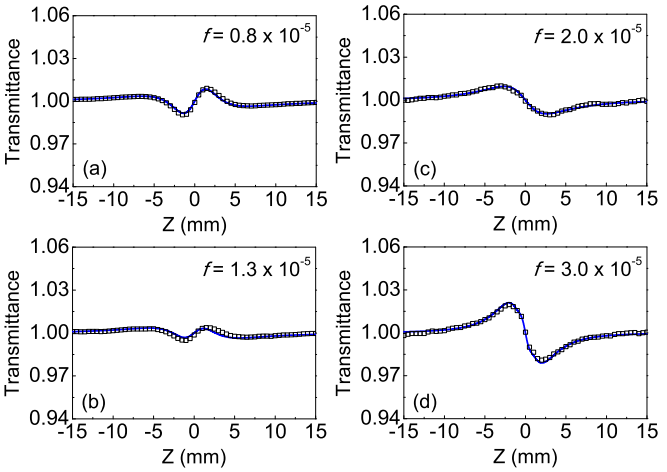

FIG. 2. (Color online) Typical *closed-aperture* Z-scan traces obtained at 532 nm for different NP volume fractions f. Negative values of Z correspond to locations of the sample between the focusing lens and its focal plane. The solid lines are guides to the eyes. Laser peak intensity: 5.0 GW/cm^2.

procedure allows obtaining a narrow size distribution of NPs as demonstrated in [13,21] and by the narrow spectrum of Fig. 1. In addition, the spectrum of pure acetone is shown to assure that the band centered at ≈400 nm (linewidth ≈ 50 nm) is due to the surface plasmon resonance associated with the NPs.

The Z-scan technique [22] was used for characterization of the samples. For the measurements the sample was moved along the beam propagation direction (Z axis) in the region where the laser beam is focused. Measurements of the transmitted beam intensity through a small aperture placed in front of a photodetector in the far-field region provide the NL refractive index value (*closed-aperture* scheme). When all the light transmitted through the sample is detected, the NL absorption coefficient can be determined (*open-aperture* scheme) scanning the sample in the focus region and measuring the transmitted intensity by a detector positioned in the far-field region. For both Z-scan schemes the laser beam was focused by a 5-cm focal distance lens, producing a beam waist of 20 μm at the focus. The detected signals were processed by boxcar integrators and computer. To improve the signal-to-noise ratio in the Z-scan experiment a reference channel was used as in [23]. Carbon disulfide (CS_2) with NL refractive index equal to $+3.1 \times 10^{-14}$ cm^2/W [22] was the reference standard for calibration of the measurements.

Figure 2 shows *closed-aperture* Z-scan traces corresponding to four f values. The colloid inside a 1-mm-long quartz cell was scanned along the Z axis using a translation stage. Figures 2(a) and 2(b) show profiles that indicate positive NL refractive index for $f = 0.8 \times 10^{-5}$ and $f = 1.3 \times 10^{-5}$, respectively. The normalized peak-to-valley transmittance change, $|\Delta T_{PV}|$, is smaller in Fig. 2(b) than in Fig. 2(a) because the NPs contribute to the NL refractive index with the opposite sign than acetone that has $n_2 = +2.16 \times 10^{-15}$ cm^2/W [24]. Figures 2(c) and 2(d), corresponding to $f \geqslant 2 \times 10^{-5}$, indicate that the NL refractive index of the colloid became negative because the silver NPs dominate the NL response. For small laser intensities ($I \leqslant 2.0$ GW/cm^2) we determined n_2 for different f values using the expression $|\Delta T_{PV}| = 0.406 k L_{\text{eff}} n_2 I$ from Ref. [22], where $k = 2\pi n_0/\lambda$, $L_{\text{eff}} = [1 - \exp(-\alpha_0 L)]/\alpha_0$, L is the sample length, α_0 is the linear absorption coefficient, and λ is the laser wavelength. The sign reversal of n_2 as a function of f was observed for all intensities used. However, no sign reversal of n_2 was observed fixing f and changing I for the whole range of f values.

Figure 3(a) shows additional features in the *closed-aperture* Z-scan profiles due to HON for $I > 6.0$ GW/cm^2 and Fig. 3(b) shows *open-aperture* profiles for various laser intensities. The solid curves were obtained following the procedure of [13] as described below. After each Z-scan experiment no changes were observed in the linear absorption spectrum indicating that the energy of the laser pulses did not change the samples'

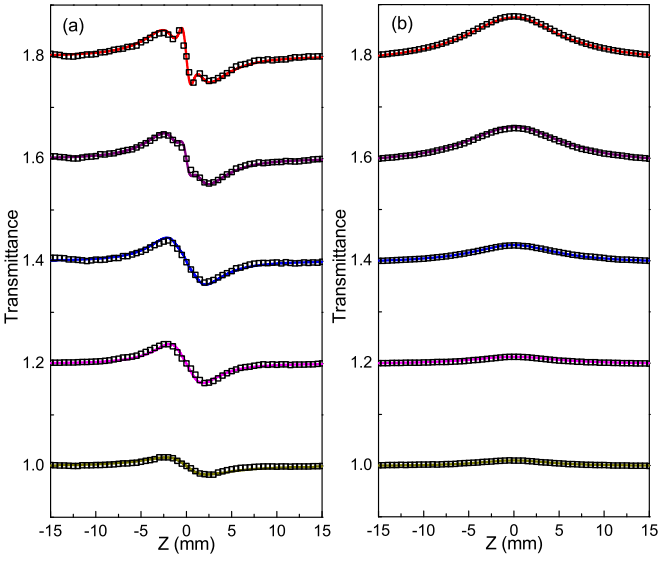

FIG. 3. (Color online) Normalized Z-scan traces obtained for different laser peak intensities: (a) *Closed-aperture* scheme and (b) *open-aperture* scheme. From bottom to top, the curves correspond to 2, 4, 6, 8, and 9 GW/cm^2. Volume fraction: $f = 5.0 \times 10^{-5}$. The curves were normalized and shifted in the vertical to prevent overlap.

characteristics. The NL experiments were repeated more than one time with each sample and the results were reproduced.

To analyze the experimental results we plotted $|\Delta T_{PV}|/I$ versus I following the same procedure as [13]. For $f < 0.8 \times 10^{-5}$ the ratio $|\Delta T_{PV}|/I$ remains constant for intensities up to 10 GW/cm^2, indicating negligible contributions of $\chi_{\text{eff}}^{(2N+1)}$ $(N > 1)$. For $f \approx 1.3 \times 10^{-5}$, the ratio $|\Delta T_{PV}|/I$ presents linear dependence with the laser intensity and from the slope of the straight line we determined $n_4 \propto \text{Re}\chi_{\text{eff}}^{(5)}$ [13]. For $f \geqslant 2.0 \times 10^{-5}$ the laser intensity dependence of $|\Delta T_{PV}|/I$ is a polynomial function that allows obtaining the refractive indices associated to NL susceptibilities up to the seventh order. The polynomial fit was performed based on 20 experimental points corresponding to intensities between 2 and 10 GW/cm^2, for each f value, with a measurement uncertainty of 15% due to the laser intensity fluctuations. The algorithm used to obtained the best fit was a combination of the Levenberg-Marquardt and the least-squares minimum method with determination coefficient, $R^2 > 0.95$. For instance, when $f = 2.5 \times 10^{-5}$ and $I = 9.0$ GW/cm^2 we determined $n_2 = -1.1 \times 10^{-15}$ cm^2/W, $n_4 = +6.9 \times 10^{-25}$ cm^4/W^2, and $n_6 = -1.1 \times 10^{-34}$ cm^6/W^3. Notice that the values of n_2, n_4, n_6 and α_2, α_4, α_6 obtained from the polynomial fit were used to adjust the experimental Z-scan profiles shown in Figs. 2 and 3 with good agreement. It is important to remark that if the NL coefficients values used (including their signs) were different, the Z-scan traces would present other profiles.

The ratio $|\Delta T_{PV}|/I$ also exhibited a polynomial dependence with I in the *open-aperture* experiments and from the results shown in Fig. 3(b) we obtained α_i $(i = 2, 4, 6)$ for different values of f. For example, for $f = 5.0 \times 10^{-5}$, we have $\alpha_2 = -4.9 \times 10^{-10}$ cm/W, $\alpha_4 = +1.4 \times 10^{-19}$ cm^3/W^2, and $\alpha_6 = -1.7 \times 10^{-29}$ cm^5/W^3.

Figure 4 shows that n_2, n_4, α_2, and α_4 present linear dependence with f. Notice that for $f \approx 1.6 \times 10^{-5}$ we have $n_2 = 0$ but $n_4 = +3.2 \times 10^{-25}$ cm^4/W^2. This result does not violate the powers series of the NL polarization and opens routes for exploitation of unique effects considering that under the conditions identified here $\text{Re}\chi_{\text{eff}}^{(5)}$ is the lowest-order NL refractive response.

In addition, spatial cross-phase modulation experiments were performed to exploit the response of the MDNC with

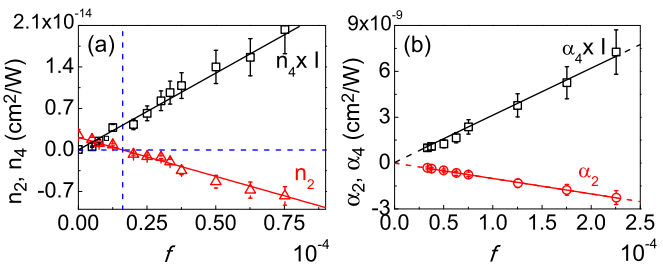

FIG. 4. (Color online) Dependence of the effective third-order coefficients ($n_2 \propto \text{Re}\chi_{\text{eff}}^{(3)}$ and $\alpha_2 \propto \text{Im}\chi_{\text{eff}}^{(3)}$) and the effective fifth-order coefficients ($n_4 \propto \text{Re}\chi_{\text{eff}}^{(5)}$ and $\alpha_4 \propto \text{Im}\chi_{\text{eff}}^{(5)}$) versus the NP volume fraction, f: (a) n_2 and $n_4 I$; (b) α_2 and $\alpha_4 I$. Laser peak intensity: $I = 9.0$ GW/cm^2.

adjustable f values. The laser beam was split into probe and pump beams with intensity ratio 1:10. The probe beam was weak in order to not induce NL changes in the beam profile. The pump and probe beams were aligned to counterpropagate along the sample and a careful adjustment of the spatial and temporal overlap between the pulses was made. The measured beams' waists were ≈100 μm with Rayleigh lengths of ≈6 cm. The beams' profiles were analyzed using a CCD camera.

Figures 5(a)–5(c) show the probe beam profiles when the pump beam with 2.0 GW/cm^2 is present; the results presented correspond to $f = 0.5 \times 10^{-5}$, 1.6×10^{-5}, and 2.5×10^{-5}, respectively. We analyzed the spatial profile of the probe beam as an intensity matrix; the curves in Figs. 5(d)–5(f) represent column matrix components passing through the axis of the probe beam exhibiting the beam intensity versus the radial coordinate. As expected, we observed spatial broadening of the probe beam due to the presence of the pump beam that induces spatial cross-phase modulation. Moreover, additional spatial frequencies were generated due to the spatial-modulation instability (SMI) of the probe beam induced by the pump beam, as noticed by the feature induced in the center of the probe beam profile. Due to the f values used, Figs. 5(d) and 5(e) exhibit the SMI effect due to only $\chi_{\text{eff}}^{(3)}$ and only $\chi_{\text{eff}}^{(5)}$, respectively; Fig. 5(f) illustrates the simultaneous influence of $\chi_{\text{eff}}^{(3)}$ and $\chi_{\text{eff}}^{(5)}$. Figures 5(g)–5(i) show the numerical results obtained from Eqs. (3) and (4).

To understand the results reported here we developed an extension of the Maxwell-Garnet model [25] including the contributions of the third- and fifth-order susceptibilities. The quasistatic approximation was assumed because the NP diameters are smaller than the λ value. Accordingly, for $f \ll 1$ and optical electric field, $\boldsymbol{E}_0$, the induced polarization can be written as $\boldsymbol{P} = \boldsymbol{P_h} + \frac{1}{V}\sum_{i=1}^{N_p} \boldsymbol{p_i}$, where $\boldsymbol{P}_h$ is the host polarization, N_p is the number of NPs inside the volume V, and $\boldsymbol{p}_i = \varepsilon_h \sigma_i \boldsymbol{E}_0$ is the induced dipole moment of each NP; σ_i is the NP polarizability given by $\sigma_i = 3v_i(\frac{\varepsilon_{np}-\varepsilon_h}{\varepsilon_{np}+2\varepsilon_h})$, where ε_{np} (ε_h) is the dielectric function of the NPs (host) and v_i is the volume of the NP. The dielectric functions can be expressed as a sum of the linear and NL contributions such that $\varepsilon_{h,np} = \varepsilon_{h,np}^{(L)} + \varepsilon_{h,np}^{(NL)}$, where the NL terms are given by $\varepsilon_{np}^{(NL)} = \frac{3}{4}\chi_{np}^{(3)}\langle|\boldsymbol{E}_{np}|^2\rangle + \frac{5}{8}\chi_{np}^{(5)}(\langle|\boldsymbol{E}_{np}|^2\rangle)^2$ and $\varepsilon_h^{(NL)} = \frac{3}{4}\chi_h^{(3)}\langle|\boldsymbol{E}_0|^2\rangle$, with $\chi_{np}^{(i)}, i = 3, 5$, and $\chi_h^{(3)}$ being the ith NL susceptibility of the NPs and the third-order susceptibility of the host, respectively. The expression $\langle|\boldsymbol{E}_{np}|^2\rangle = |\eta|^2|\boldsymbol{E}_0|^2$ represents the mean squared modulus of the electric field inside the NP and $\eta = 3\varepsilon_h/(\varepsilon_{np} + 2\varepsilon_h)$ is the local field factor. The effective NL susceptibilities are determined expanding the polarizability up to second order in $|\boldsymbol{E}_0|^2$ to obtain

$$\chi_{\text{eff}}^{(3)} = f\, L^2|L|^2\chi_{np}^{(3)} + \chi_h^{(3)}, \tag{1}$$

$$\chi_{\text{eff}}^{(5)} = f\, L^2|L|^4\chi_{np}^{(5)} - \frac{6}{10} f\, L^3|L|^4\left(\chi_{np}^{(3)}\right)^2 - \frac{3}{10} f\, L|L|^6\left|\chi_{np}^{(3)}\right|^2, \tag{2}$$

where $L = 3\varepsilon_h^{(L)}/(\varepsilon_{np}^{(L)} + 2\varepsilon_h^{(L)})$.

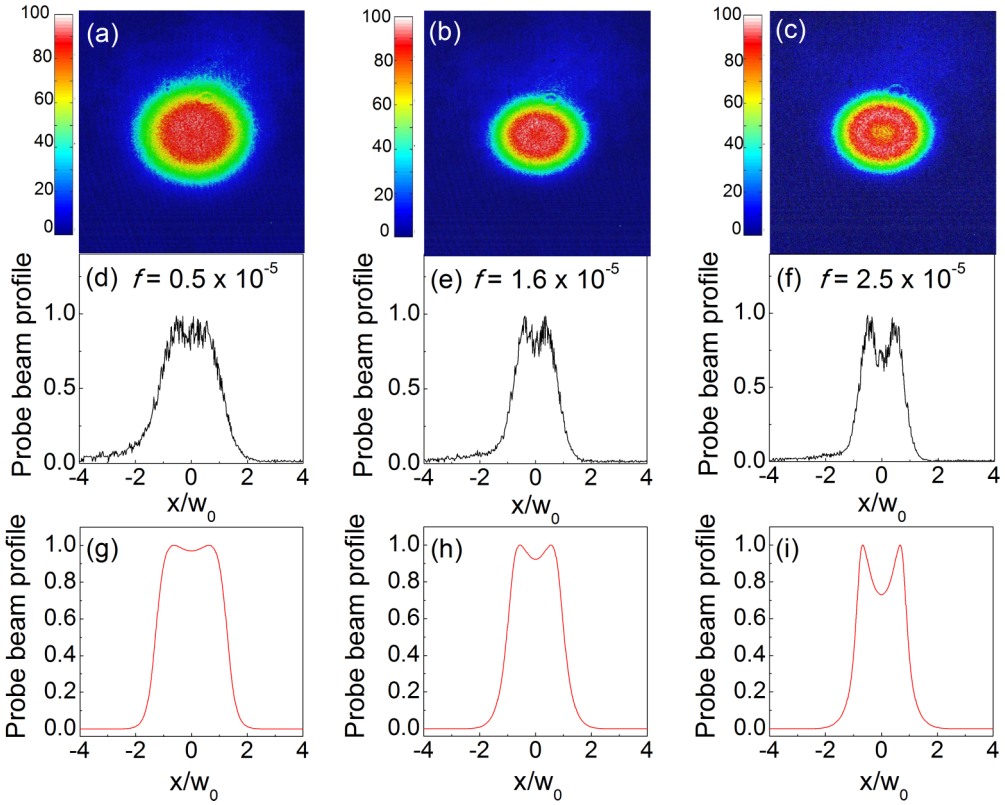

FIG. 5. (Color online) Probe beam profile in the presence of the counterpropagating pump beam: (a) $f_1 = 0.5 \times 10^{-5}$; (b) $f_2 = 1.6 \times 10^{-5}$; (c) $f_3 = 2.5 \times 10^{-5}$. Probe beam intensity versus the radial coordinate: (d) f_1; (e) f_2; (f) f_3. Numerical results using the values of n_2 and n_4 determined in the Z-scan experiments and f as in (d)–(f). Pump beam intensity 2.0 GW/cm^2; probe beam intensity: 0.2 GW/cm^2.

Equation (1) corroborates our interpretation of Fig. 2; i.e., the sign reversal of $\mathrm{Re}\chi^{(3)}_{\mathrm{eff}}$ as a function of f is due to competition between the terms containing $\mathrm{Re}\chi^{(3)}_{np}$ and $\mathrm{Re}\chi^{(3)}_{h}$ that have opposite signs. Equation (2) was derived neglecting terms proportional to $(\chi^{(3)}_h)^2$ and $(\chi^{(3)}_h\chi^{(3)}_{np})$ due to the magnitude of $\chi^{(3)}_h = +1.67 \times 10^{-21}$ (m^2/V^2) that is approximately five orders of magnitude smaller than $\chi^{(3)}_{np}$. The fifth-order susceptibility of the host was neglected in comparison with the contributions due to the NPs. It can be seen from Eq. (2) that the NPs' contributions to the direct fifth-order susceptibility, $\chi^{(5)}_{np}$ and cascade of third-order susceptibility (terms with $\chi^{(3)}_{np}$) are enhanced due to the high powers of L and $|L|$. The NL response of the NPs is attributed mainly to the s electrons in the conduction band because the energy difference between the d band and the Fermi level is $\approx$4 eV, larger than the energy of the incident photons (2.34 eV).

From Eqs. (1) and (2), we verified that $\mathrm{Im}\chi^{(3)}_{\mathrm{eff}}$ ($\mathrm{Re}\chi^{(5)}_{\mathrm{eff}}$) is negative (positive) for all values of f, in agreement with the experiments. Considering $\varepsilon^{(L)}_{np} = (0.055 + i3.455)^2$ [26] and $\varepsilon^{(L)}_{h} = (n_0)^2$, with $n_0 = 1.36$, we obtained $\chi^{(3)}_{np} = -5.9 \times 10^{-16} - i\,8.5 \times 10^{-16}$ (m^2/V^2), $\chi^{(5)}_{np} = -1.0 \times 10^{-33} - i\,1.7 \times 10^{-31}$ (m^4/V^4) and $\chi^{(5)}_{\mathrm{eff}} = +3.7 \times 10^{-38} + i\,3.3 \times 10^{-37}$ (m^4/V^4). For $f = 1.6 \times 10^{-5}$ we have $n_2 \propto \mathrm{Re}\chi^{(3)}_{\mathrm{eff}} = 0$ and $n_4 \propto \mathrm{Re}\chi^{(5)}_{\mathrm{eff}} \neq 0$ due to the cascade process associated with $(\chi^{(3)}_{np})^2$ and $|\chi^{(3)}_{np}|^2$, and to the direct process described by $\chi^{(5)}_{np}$. Moreover, $\alpha_2 = -1.6 \times 10^{-10}$ cm/W and $\alpha_4 = +2.2 \times 10^{-20}$ cm^3/W^2 are very small indicating that the MDNC presents essentially a refractive nonlinearity for $f = 1.6 \times 10^{-5}$.

The cross-phase modulation experiment can be described by a pair of coupled equations that relate the pump and probe beams as

$$-\frac{\partial A_1}{\partial z} - \frac{i}{2k}\left(\frac{\partial^2 A_1}{\partial x^2} + \frac{\partial^2 A_1}{\partial y^2}\right) = \frac{ikn_2}{n_0}(|A_1|^2 + 2|A_2|^2)A_1 + \frac{ikn_4}{n_0}(|A_1|^4 + 6|A_1|^2|A_2|^2 + 3|A_2|^4)A_1, \quad (3)$$

$$\frac{\partial A_2}{\partial z} - \frac{i}{2k}\left(\frac{\partial^2 A_2}{\partial x^2} + \frac{\partial^2 A_2}{\partial y^2}\right) = \frac{ikn_2}{n_0}(|A_2|^2 + 2|A_1|^2)A_2 + \frac{ikn_4}{n_0}(|A_2|^4 + 6|A_1|^2|A_2|^2 + 3|A_1|^4)A_2, \quad (4)$$

where A_1 and A_2 are the slowly varying envelope amplitude of the pump and probe beams, respectively; $k = 2\pi n_0/\lambda$, and x and y are the transverse coordinates.

Equations (3) and (4) were solved using the split-step method and considering only one transverse dimension due

to the cylindrical symmetry of the beams. The numerical results, considering the values of n_2 and n_4, determined in the Z-scan experiments, are shown in Figs. 5(g)–5(i) where a good agreement with the experimental results is observed. The amplitude of the signal shown in Fig. 5(b) is approximately threefold smaller than the signals corresponding to 5(a) and 5(c) because it is due to the quintic nonlinearity only. The reduction of the probe beam intensity in the center of the spatial profile is well described by the theoretical model. The contribution due to the positive value of n_4 is noticed by the narrower spatial profile shown in Figs. 5(b) and 5(c). We emphasize that the experimental results shown in Figs. 5(b) and 5(e) represent a demonstration of SMI due to the fifth-order susceptibility in a system with $n_2 = 0$ and $n_4 \neq 0$.

IV. SUMMARY

In summary, we demonstrated the conditions under which the real part of the effective third-order susceptibility of a MDNC can be suppressed and the NL refractive response is dominated by the fifth-order nonlinearity. The present experiments demonstrate a procedure for managing cubic-quintic composites in order to develop systems with dominant quintic refractive nonlinearity and negligible cubic refraction. As an application we demonstrated the spatial-modulation instability due to the fifth-order NL refraction. From the basic point of view such engineered MDNC offer the possibility for practical realization of some mathematical models proposed in the literature [7]. Of course, because of the frequency-dependent mismatch between the dielectric functions of the NPs and the host, as well as the excitation of localized surface plasmons (LSPs) in the NPs, the NL susceptibilities of the nanocomposites may be further enhanced by using laser frequencies near resonance with the LSP frequency.

ACKNOWLEDGMENTS

We acknowledge financial support from the Brazilian agencies Conselho Nacional de Desenvolvimento Cientifico e Tecnológico (CNPq) and the Fundação de Amparo à Ciência e Tecnologia do Estado de Pernambuco (FACEPE). The work was performed in the framework of the National Institute of Photonics (INCT de Fotônica) project and PRONEX/CNPq/FACEPE.

[1] N. Bloembergen, *Nonlinear Optics* (W. A. Benjamin, New York, 1965).

[2] L. H. Acioli, A. S. L. Gomes, J. R. R. Leite, and C. B. de Araújo, IEEE Quantum Electron. **26**, 1277 (1990); G. Boudebs, S. Cherukulappurath, H. Leblond, J. Troles, F. Smektala, and F. Sanchez, Opt. Commun. **219**, 427 (2003); G. Stegeman, D. G. Papazoglou, R. Boyd, and S. Tzortzakis, Opt. Express **19**, 6387 (2011); M. Bache, F. Eilenberger, and S. Minardi, Opt. Lett. **37**, 4612 (2012); B. Borchers, C. Brée, S. Birkholz, A. Demircan, and G. Steinmeyer, *ibid.* **37**, 1541 (2012); X. Liu, Y. Adachi, Y. Tomita, J. Oshima, T. Nakashima, and T. Kawai, Opt. Express **20**, 13457 (2012).

[3] L. H. Acioli, A. S. L. Gomes, and J. R. R. Leite, Appl. Phys. Lett. **53**, 1788 (1988); J. Arabat and J. Etchepare, J. Opt. Soc. Am. B **10**, 2377 (1993); K. D. Moll, D. Homoelle, A. L. Gaeta, and R. W. Boyd, Phys. Rev. Lett. **88**, 153901 (2002); Y.-F. Chen, K. Beckwitt, F. W. Wise, B. G. Aitken, J. S. Sanghera, and I. D. Aggarwal, J. Opt. Soc. Am. B **23**, 347 (2006); V. Vaičaitis, V. Jarutis, and D. Pentaris, Phys. Rev. Lett. **103**, 103901 (2009).

[4] K. Dolgaleva, H. Shin, and R. W. Boyd, Phys. Rev. Lett. **103**, 113902 (2009); J. Jayabalan, J. Opt. Soc. Am. B **28**, 2448 (2011); C. Brée, A. Demircan, and G. Steinmeyer, Phys. Rev. Lett. **106**, 183902 (2011); N. J. Dawson and J. H. Andrews, J. Phys. B: At. Mol. Opt. Phys. **45**, 035401 (2012); B. B. Zhou, A. Chong, F. W. Wise, and M. Bache, Phys. Rev. Lett. **109**, 043902 (2012); H. Zheng, X. Zhang, Z. Zhang, Y. Tian, H. Chen, C. Li, and Y. Zhang, Sci. Rep. **3**, 1885 (2013).

[5] H. Michinel, M. J. Paz-Alonso, and V. M. Pérez-García, Phys. Rev. Lett. **96**, 023903 (2006).

[6] E. L. Falcão-Filho, C. B. de Araújo, G. Boudebs, H. Leblond, and V. Skarka, Phys. Rev. Lett. **110**, 013901 (2013); E. D'Asaro, S. Heidari-Bateni, A. Pasquazi, G. Assanto, J. Gonzalo, J. Solis, and C. N. Afonso, Opt. Express **17**, 17150 (2009).

[7] J. Zeng and B. A. Malomed, Phys. Rev. A **85**, 023824 (2012); Phys. Rev. E **86**, 036607 (2012); R. M. Caplan, R. Carretero-González, P. G. Kevrekidis, and B. A. Malomed, Math. Comput. Simul. **82**, 1150 (2012); G. Fibich, N. Gavish, and X.-P. Wang, Physica D **231**, 55 (2007); C. Rogers, B. Malomed, J. H. Li, and K. W. Chow, J. Phys. Soc. Jpn. **81**, 094005 (2012); M. Crosta, A. Fratalocchi, and S. Trillo, Phys. Rev. A **84**, 063809 (2011).

[8] V. Vaičaitis, V. Jarutis, K. Steponkevičius, and A. Stabinis, Phys. Rev. A **87**, 063825 (2013); G. Burlak and B. A. Malomed, Phys. Rev. E **88**, 062904 (2013); P. A. Tsilifis, P. G. Kevrekidis, and V. M. Rothos, J. Phys. A: Math. Theor. **47**, 035201 (2014).

[9] H. Ma and C. B. de Araújo, Phys. Rev. Lett. **71**, 3649 (1993); S. Wu, X.-C. Zhang, and R. L. Fork, Appl. Phys. Lett. **61**, 919 (1992); Y. Zhang, A. W. Brown, and M. Xiao, Phys. Rev. Lett. **99**, 123603 (2007); Y. Zhang and M. Xiao, *Multi-Wave Mixing Processes: From Ultrafast Polarization Beats to Electromagnetically Induced Transparency* (Springer, Berlin, 2009).

[10] C. Hang, Y. Li, L. Ma, and G. Huang, Phys. Rev. A **74**, 012319 (2006).

[11] H. Kang, G. Hernandez, and Y. Zhu, Phys. Rev. Lett. **93**, 073601 (2004).

[12] Y. Zhang, U. Khadka, B. Anderson, and M. Xiao, Phys. Rev. Lett. **102**, 013601 (2009).

[13] E. L. Falcão-Filho, C. B. de Araújo, and J. J. Rodrigues, Jr., J. Opt. Soc. Am. B **24**, 2948 (2007); E. L. Falcão-Filho, R. Barbosa-Silva, R. G. Sobral-Filho, A. M. Brito-Silva, A. Galembeck, and C. B. de Araújo, Opt. Express **18**, 21636 (2010).

[14] G. S. He, W.-C. Law, A. Baev, S. Liu, M. T. Swihart, and P. N. Prasad, J. Chem. Phys. **138**, 024202 (2013).

[15] Y. Zhang, F. Wen, Y.-R. Zhen, P. Nordlander, and N. J. Halas, Proc. Natl. Acad. Sci. USA **110**, 9215 (2013).

[16] J. A. Scholl, A. L. Koh, and J. A. Dionne, Nature **483**, 421 (2012).
[17] T. Utikal, T. Zentgraf, T. Paul, C. Rockstuhl, F. Lederer, M. Lippitz, and H. Giessen, Phys. Rev. Lett. **106**, 133901 (2011).
[18] M. Kauranen and A. V. Zayats, Nat. Photonics **6**, 737 (2012).
[19] M. Centurion, M. A. Porter, P. G. Kevrekidis, and D. Psaltis, Phys. Rev. Lett. **97**, 033903 (2006); J. Fujioka, E. Cortés, R. Pérez-Pascual, R. F. Rodrígues, A. Espinosa, and B. A. Malomed, Chaos **21**, 033120 (2011); F. Kh. Abdullaev, P. G. Kevrekidis, and M. Salerno, Phys. Rev. Lett. **105**, 113901 (2010).
[20] P. C. Lee and D. Meisel, J. Phys. Chem. **86**, 3391 (1982).
[21] A. M. Brito-Silva, L. A. Gómez, C. B. de Araújo, and A. Galembeck, J. Nanomater. **2010**, 142897 (2010); L. A. Gómez, C. B. de Araújo, A. M. Brito-Silva, and A. Galembeck, Appl. Phys. B **92**, 61 (2008); J. Opt. Soc. Am. B **24**, 2136 (2007); H. Zeng, X.-W. Du, S. C. Singh, S. A. Kulinich, S. Yang, J. He, and W. Cai, Adv. Funct. Mater. **22**, 1333 (2012).
[22] M. Sheik-Bahae, A. A. Said, T.-H. Wei, D. J. Hagan, and E. W. Van Stryland, IEEE J. Quantum Electron. **26**, 760 (1990).
[23] H. Ma, A. S. L. Gomes, and C. B. de Araújo, Appl. Phys. Lett. **59**, 2666 (1991).
[24] R. L. Sutherland, *Handbook of Nonlinear Optics* (Dekker, New York, 1996).
[25] J. E. Sipe and R. W. Boyd, Phys. Rev. A **46**, 1614 (1992).
[26] P. B. Johnson and R. W. Christy, Phys. Rev. B **6**, 4370 (1972).